Electronic Supplementary Information

A noble-metal-free nanocatalyst for highly efficient and complete hydrogen evolution from $N_2H_4BH_3$

Qilu Yao,[a] Zhang-Hui Lu,[*,a] Rui Zhang,[b] Shiliang Zhang,[a] Xiangshu Chen[*,a] and Hai-Long Jiang[b]

[a]*Institute of Advanced Materials (IAM), College of Chemistry and Chemical Engineering, Jiangxi Normal University, Nanchang, 330022, P.R. China*

[b]*Hefei National Laboratory for Physical Sciences at the Microscale, Collaborative Innovation Center of Suzhou Nano Science and Technology, Department of Chemistry, University of Science and Technology of China, Hefei, Anhui 230026, P.R. China*

E-mail: luzh@jxnu.edu.cn, cxs66cn@jxnu.edu.cn

Table S1 Catalysts composition determined by inductively coupled plasma atomic emission spectroscopic (ICP-AES).

Catalysts	Cu (wt%)	Ni (wt%)	Mo (wt%)	Cu/Ni/Mo (atomic ratio)
CuMo	26.82	0	39.64	1.01/~/0.99
$Cu_{0.8}Ni_{0.2}Mo$	21.04	5.03	40.98	0.79/0.20/1.01
$Cu_{0.6}Ni_{0.4}Mo$	15.74	10.01	40.51	0.59/0.41/1.00
$Cu_{0.5}Ni_{0.5}Mo$	13.48	12.39	40.29	0.50/0.50/1.00
$Cu_{0.4}Ni_{0.6}Mo$	10.70	14.93	39.47	0.41/0.61/0.98
$Cu_{0.3}Ni_{0.7}Mo$	8.20	17.67	40.29	0.30/0.71/0.99
$Cu_{0.2}Ni_{0.8}Mo$	6.08	19.83	40.34	0.22/0.79/0.99
NiMo	0	24.58	40.30	~/1.00/1.00

Table S2 Catalytic activities for hydrogen generation from hydrazine brane catalyzed by different catalysts.

Catalysts	$n(H_2+N_2)/nN_2H_4BH_3$	t/min	TOF/h^{-1}
$Cu_{0.4}Ni_{0.6}Mo$	6	13.9	108
$Fe_{0.4}Ni_{0.6}Mo$	6	15.78	95
$Co_{0.4}Ni_{0.6}Mo$	5.57	15.26	92
$Cu_{0.4}Co_{0.6}Mo$	4.37	14.28	79
$Fe_{0.4}Co_{0.6}Mo$	3.81	33.21	30
$Cu_{0.4}Fe_{0.6}Mo$	3	0.7	-
NiMo	5.14	18.1	72
$Cu_{0.4}Ni_{0.6}$	3.3	6.3	-
CuMo	3.3	6.9	-
Cu	3.0	8.4	-
Ni	3.0	4.5	-

Table S3 Catalytic activities for the dehydrogenation of $N_2H_4BH_3$ catalyzed by different catalysts.

Catalysts	T (K)	$n(H_2+N_2)/n(N_2H_4BH_3)$	TOF (h^{-1})	Ref.
$Rh_{0.8}Ni_{0.2}$@CeO_x/rGO	323	6.0	666.7[a]	S1
$Ni_{0.6}Pt_{0.4}$/MSC-30	303	5.95	661.7[a]	S4
$Ni_{0.9}Pt_{0.1}$/graphene	323	6.0	240[a]	S2
$Ni_{0.9}Pt_{0.1}$-CeO_2	323	5.74	234[a]	S3
$Cu_{0.4}Ni_{0.6}Mo$	323	6	108[a]	This work
Rh_4Ni NPs	323	5.8	90.0[b]	S5
Ni@(Rh_4Ni-alloy)/Al_2O_3	323	5.74	72.0[a]	S6
$Ni_{0.77}Ru_{0.23}$ NPs	323	4.0	23.3[a]	S7
$Ni_{0.89}Pt_{0.11}$ NPs	323	5.79	18.0[a]	S8
$Ni_{0.89}Rh_{0.11}$ NPs	323	5.1	9.9[a]	S7
$Ni_{0.89}Ir_{0.11}$ NPs	323	4.9	9.5[a]	S7
Ni_5@Pt	323	4.4	2.3[a]	S9

[a]*The total TOF values were calculated according to the original data provided by the reports.*
[b]*The total TOF values were provided by the reports.*

Calculation method for TOF

The turn over frequency (*TOF*) reported in this work is an apparent *TOF* value based on the number of metal (Cu + Ni + Mo) atoms in catalysts, which is calculated from the equation as follows:

$$TOF = \frac{nH_2}{nmetal \times t} \qquad \text{(S1)}$$

Where nH_2 is the mole number of generated H_2, *n*metal is the total mole number of Cu, Ni, and Mo in catalyst and *t* is the completed reaction time in hour.

References

S1 Z. J. Zhang, Z. H. Lu, H. L. Tan, X. S. Chen and Q. L. Yao, *J. Mater. Chem. A*, 2015, **3**, 23520-23529.

S2 Z. J. Zhang, Z. H. Lu and X. S. Chen, *ACS Sustainable Chem. Eng.*, 2015, **3**, 1255-1261.

S3 Z. J. Zhang, Y. Q. Wang, X. S. Chen and Z. H. Lu, *J. Power Sources*, 2015, **291**, 14-19.

S4 Q. L. Zhu, D. C. Zhong, U. B. Demirci and Q. Xu, *ACS Catal.*, 2014, **4**, 4261-4268.

S5 D. C. Zhong, K. Aranishi, A. K. Singh, U. B. Demirci and Q. Xu, *Chem. Commun.*, 2012, **48**, 11945-11947.

S6 C. Li, Y. Dou, J. Liu, Y. Chen, S. He, M. Wei, D. G. Evans and X. Duan, *Chem. Commun.*, 2013, **49**, 9992-9994.

S7 Ç. Çakanyıldırım, U. B. Demirci, T. Şener, Q. Xu and P. Miele, *Int. J. Hydrogen Energy*, 2012, **37**, 9722-9729.

S8 J. Hannauer, O. Akdim, U. B. Demirci, C. Geantet, J. M. Herrmann, P. Miele and Q. Xu, *Energy Environ. Sci.*, 2011, **4**, 3355-3358.

S9 D. Clémençon, J. F. Petit, U. B. Demirci, Q. Xu and P. Miele, *J. Power Sources*, 2014, **260**, 77-81.

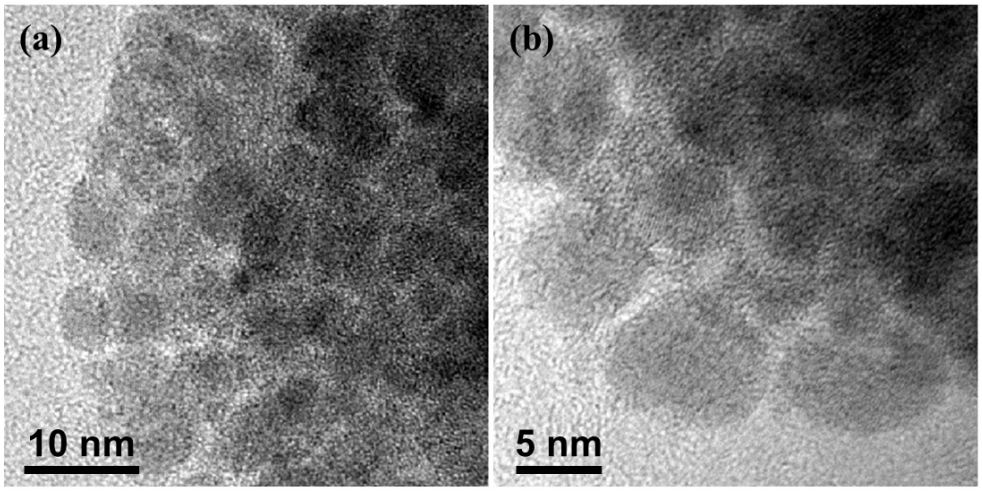

Fig. S1 (a) TEM image and (b) HRTEM image of $Cu_{0.4}Ni_{0.6}Mo$ NPs.

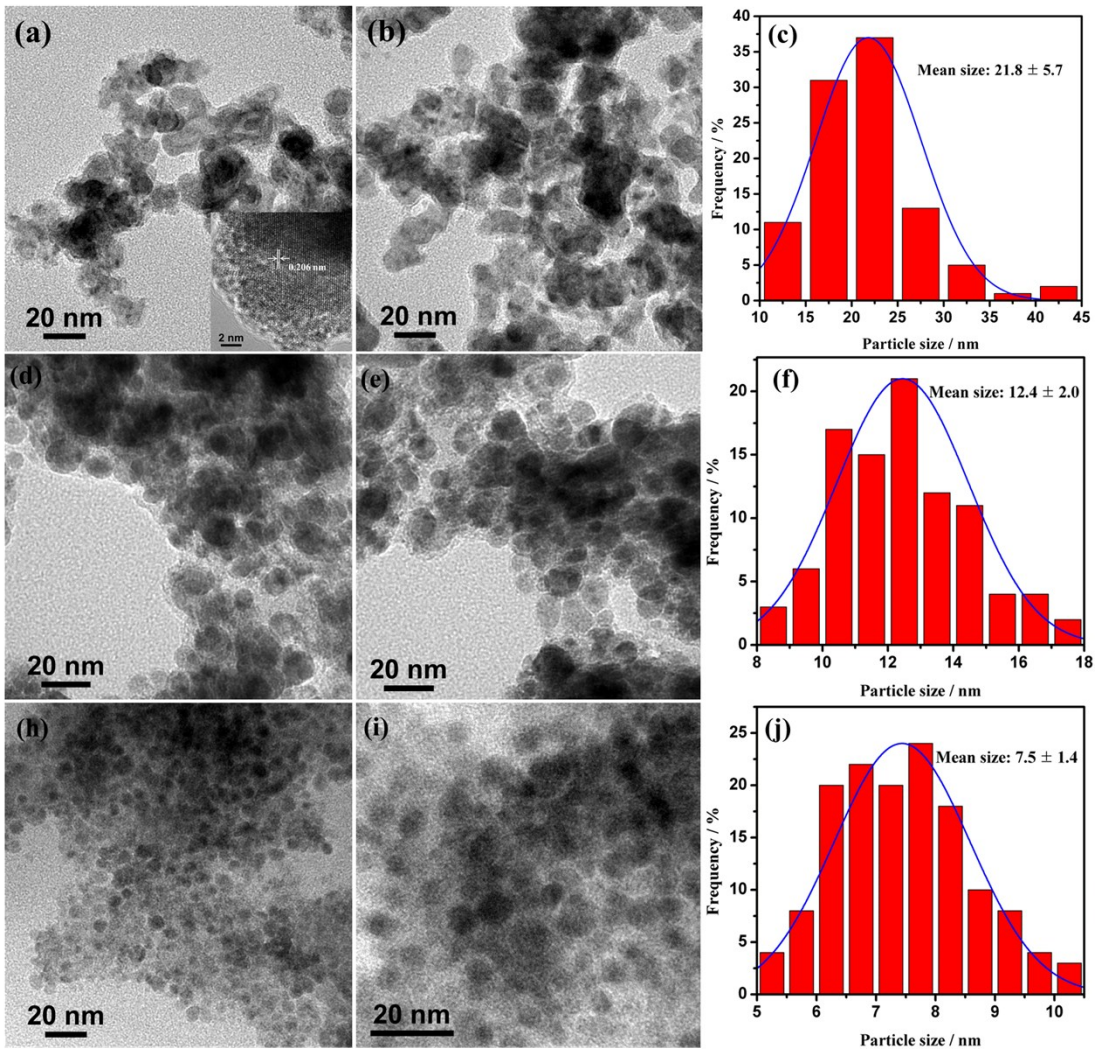

Fig. S2 TEM images and the corresponding particle size distribution of (a-b) $Cu_{0.4}Ni_{0.6}$, (d-f) $Cu_{0.4}Ni_{0.6}Mo_{0.1}$, and (h-j) $Cu_{0.4}Ni_{0.6}Mo_{0.6}$ NPs. The inset of (a) is the HRTEM image of $Cu_{0.4}Ni_{0.6}$ NPs.

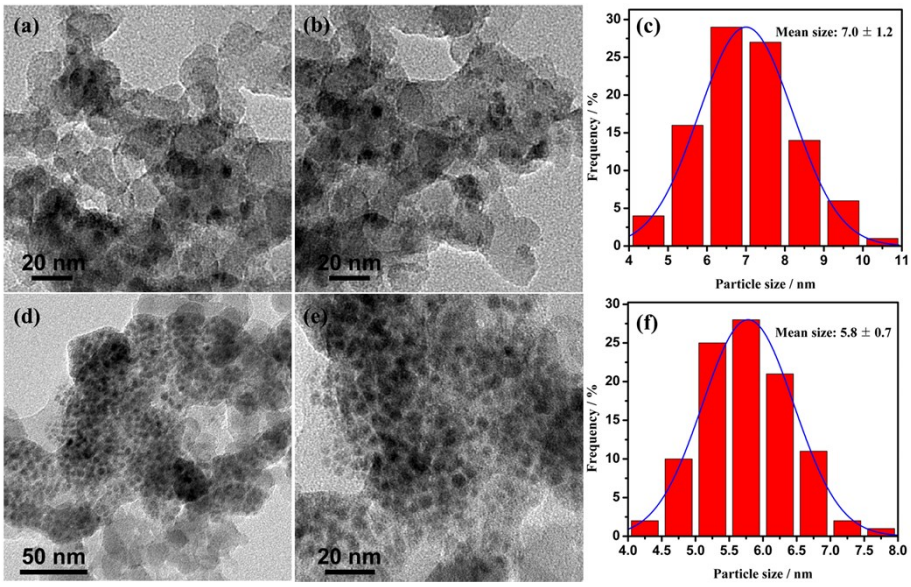

Fig. S3 TEM images and the corresponding particle size distribution of (a-c) $Cu_{0.4}Ni_{0.6}/SiO_2$ and (d-f) $Cu_{0.4}Ni_{0.6}Mo/SiO_2$ (2.0 wt%, commercial SiO_2, 200 m^2 g^{-1}, Degussa).

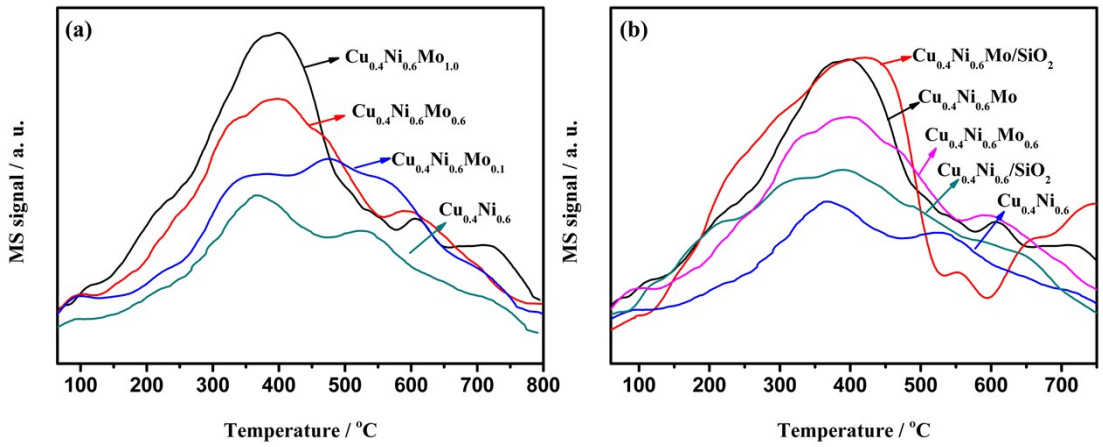

Fig. S4 CO_2-TPD mass spectra for the (a) $Cu_{0.4}Ni_{0.6}Mo_x$ (x = 0, 0.1, 0.6, and 1.0) and (b) $Cu_{0.4}Ni_{0.6}$, $Cu_{0.4}Ni_{0.6}/SiO_2$ (2.0 wt%), $Cu_{0.4}Ni_{0.6}Mo$, $Cu_{0.4}Ni_{0.6}Mo_{0.6}$, and $Cu_{0.4}Ni_{0.6}Mo/SiO_2$ (2.0 wt%, commercial SiO_2, 200 m^2 g^{-1}, Degussa).

As shown in Fig. S4a, the basic sites of the $Cu_{0.4}Ni_{0.6}Mo_x$ NPs (x = 0, 0.1, 0.6, and 1.0) tend to gradually strengthen with the increase of Mo content. The above TEM results (Fig. S2) show that the particle size of $Cu_{0.4}Ni_{0.6}Mo_x$ decreases as the Mo content increases. In addition, it is also found that the strength of basic sites of the $Cu_{0.4}Ni_{0.6}/SiO_2$ (7.0 nm, Fig. S3c) is higher than that of $Cu_{0.4}Ni_{0.6}$ (larger size, 21.8 nm, Fig. S2c). These results show that the basic sites of sample increase with the decrease of the particle size. To eliminate the effect of particle size on CO_2-TPD strength, the similar particle size of $Cu_{0.4}Ni_{0.6}/SiO_2$ (7.0 nm, Fig. S3) and $Cu_{0.4}Ni_{0.6}Mo/SiO_2$ (5.8 nm, Fig. S3) were synthesized and analyzed by CO_2-TPD measurement. As exhibited in Fig. S4b, the strength of basic sites of the $Cu_{0.4}Ni_{0.6}Mo/SiO_2$ (5.8 nm, Fig. S3), $Cu_{0.6}Ni_{0.4}Mo$ (5.9 nm, Fig. 1b), and $Cu_{0.6}Ni_{0.4}Mo_{0.6}$ (7.5 nm, Fig. S2) are higher than that of $Cu_{0.4}Ni_{0.6}/SiO_2$ (7.0 nm, Fig. S3), indicating that the introduction of Mo into $Cu_{0.4}Ni_{0.6}$ NPs can strengthen the basic sites. Therefore, it is reasonable to conclude that the strength of basic sites of catalyst is related to not only the particle size, but also the composition of the catalyst.

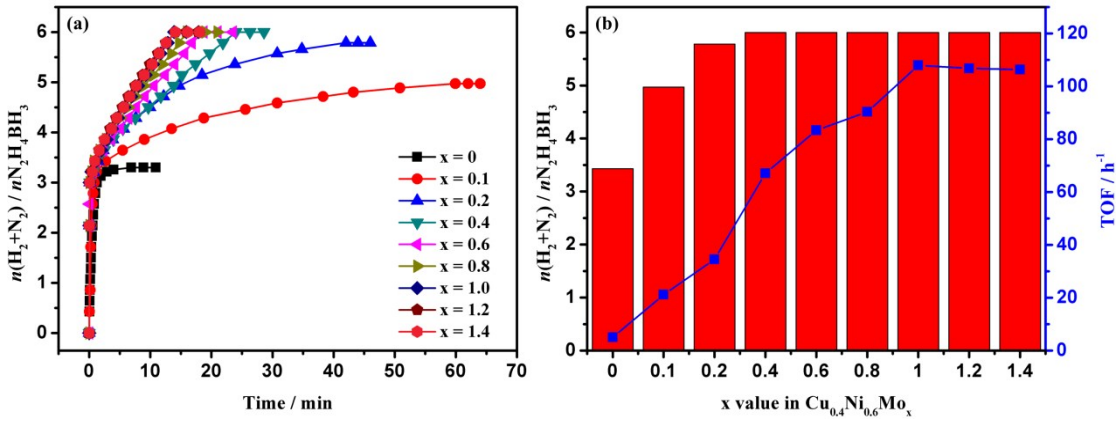

Fig. S5 (a) Time-course plots and (b) Mo-content dependence of $n(H_2 + N_2)/nNH_4BH_3$ and TOF values for the dehydrogenation of $N_2H_4BH_3$ aqueous solution (0.2 M, 5 mL) catalyzed by $Cu_{0.4}Ni_{0.6}Mo_x$ catalysts with different Mo molar contents in the presence of NaOH (2.0 M) at 323K (x = n_{Mo}/n_{Cu+Ni}; n_{Cu+Ni} = 0.1 mmol).

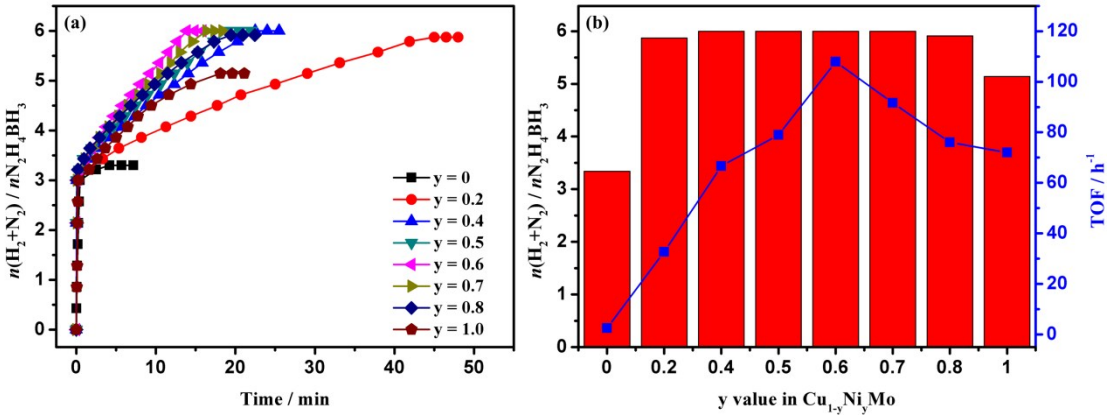

Fig. S6 (a) Time-course plots and (b) Cu/Ni compositional dependence of $n(H_2 + N_2)/nNH_4BH_3$ and TOF values for the dehydrogenation of $N_2H_4BH_3$ aqueous solution (0.2 M, 5 mL) catalyzed by $Cu_{1-y}Ni_yMo$ NPs with different compositions of Cu and Ni in the presence of NaOH (2.0 M) at 323 K ($n_{metal}/n_{N_2H_4BH_3} = 0.2$).

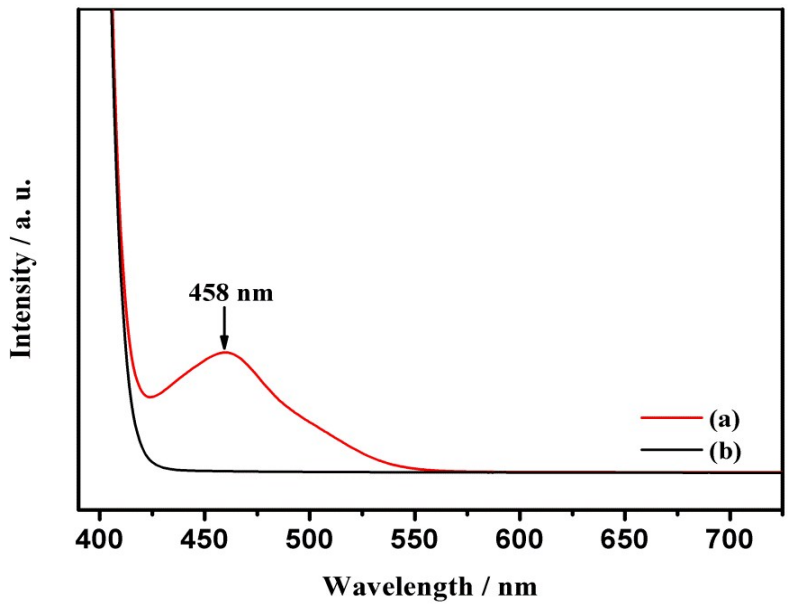

Fig. S7 UV-Vis spectra of $N_2H_4BH_3$ (a) before and (b) after the completion of $N_2H_4BH_3$ dehydrogenation reaction catalyzed by the $Cu_{0.4}Ni_{0.6}Mo$ NPs. After the catalytic reaction, the reaction solution was obtained by centrifuging the reaction suspension to separate the solution and the $Cu_{0.4}Ni_{0.6}Mo$ NPs.

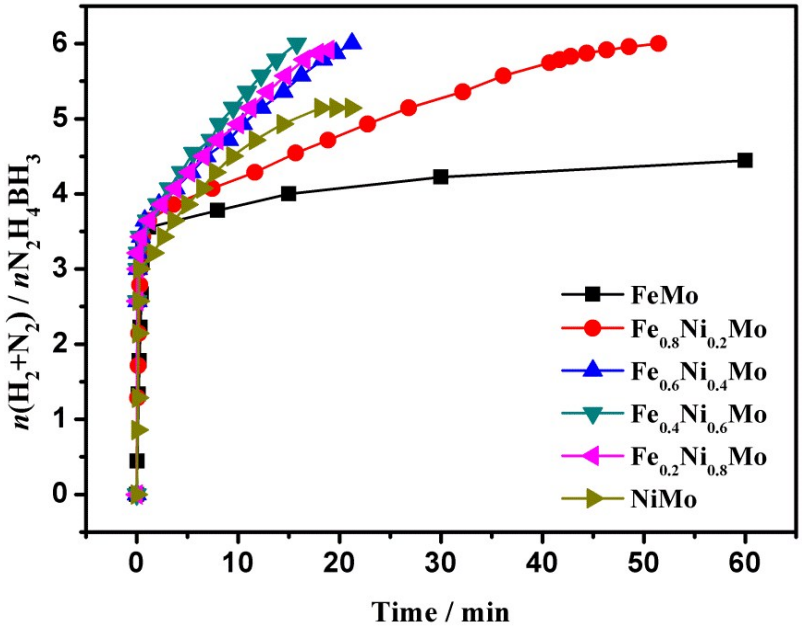

Fig. S8 Time-course plots for the dehydrogenation of $N_2H_4BH_3$ aqueous solution (0.2 M, 5 mL) catalyzed by $Fe_{1-y}Ni_yMo$ NPs with different compositions of Fe and Ni in the presence of NaOH (2.0 M) at 323 K ($n_{metal}/n_{N_2H_4BH_3}$ = 0.2).

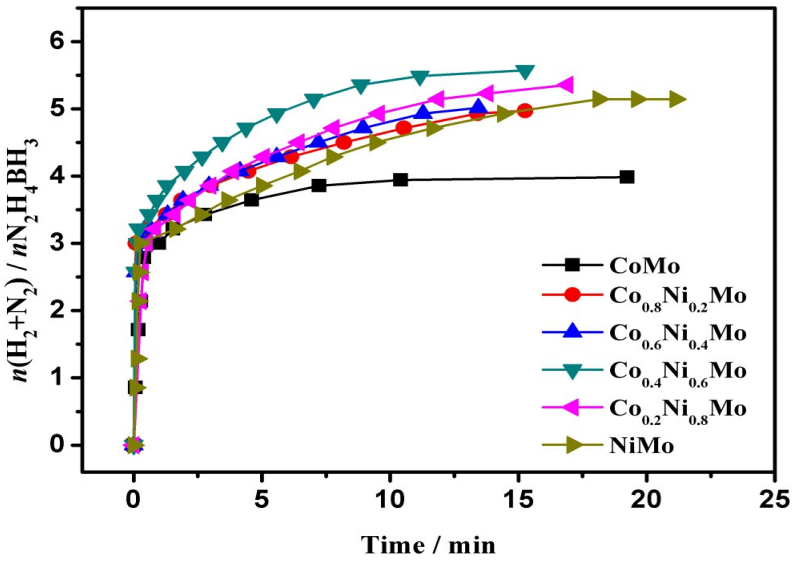

Fig. S9 Time-course plots for the dehydrogenation of $N_2H_4BH_3$ aqueous solution (0.2 M, 5 mL) catalyzed by $Co_{1-y}Ni_yMo$ NPs with different compositions of Co and Ni in the presence of NaOH (2.0 M) at 323 K ($n_{metal}/n_{N_2H_4BH_3}$ = 0.2).

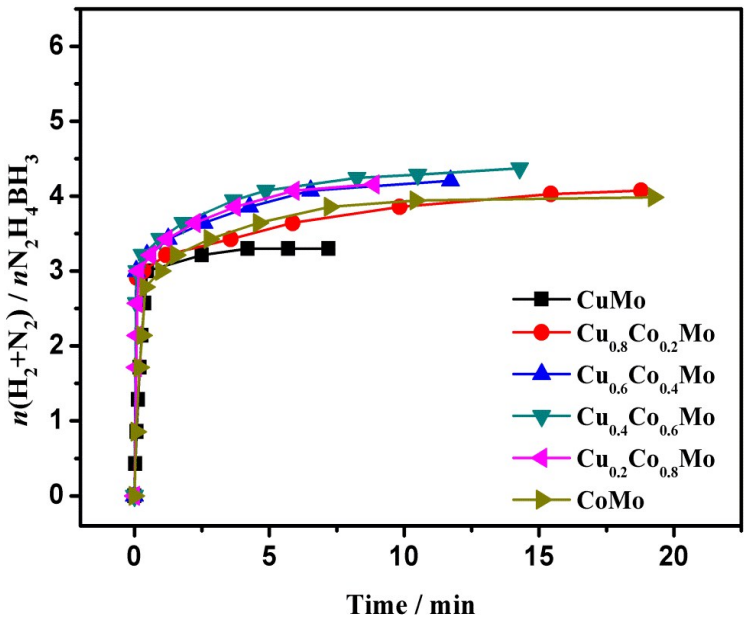

Fig. S10 Time-course plots for the dehydrogenation of $N_2H_4BH_3$ aqueous solution (0.2 M, 5 mL) catalyzed by $Cu_{1-y}Co_yMo$ NPs with different compositions of Cu and Co in the presence of NaOH (2.0 M) at 323 K ($n_{metal}/n_{N_2H_4BH_3}$ = 0.2).

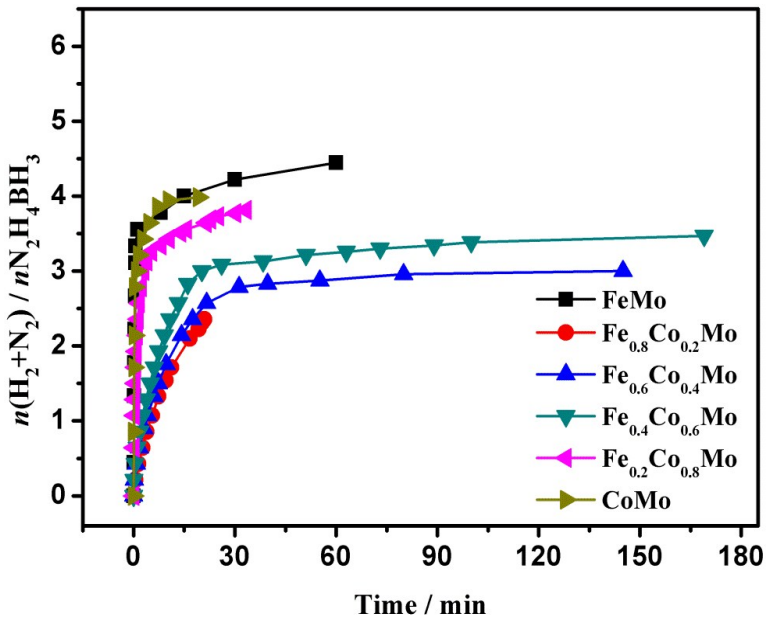

Fig. S11 Time-course plots for the dehydrogenation of $N_2H_4BH_3$ aqueous solution (0.2 M, 5 mL) catalyzed by $Fe_{1-y}Co_yMo$ NPs with different compositions of Fe and Co in the presence of NaOH (2.0 M) at 323 K ($n_{metal}/n_{N_2H_4BH_3}$ = 0.2).

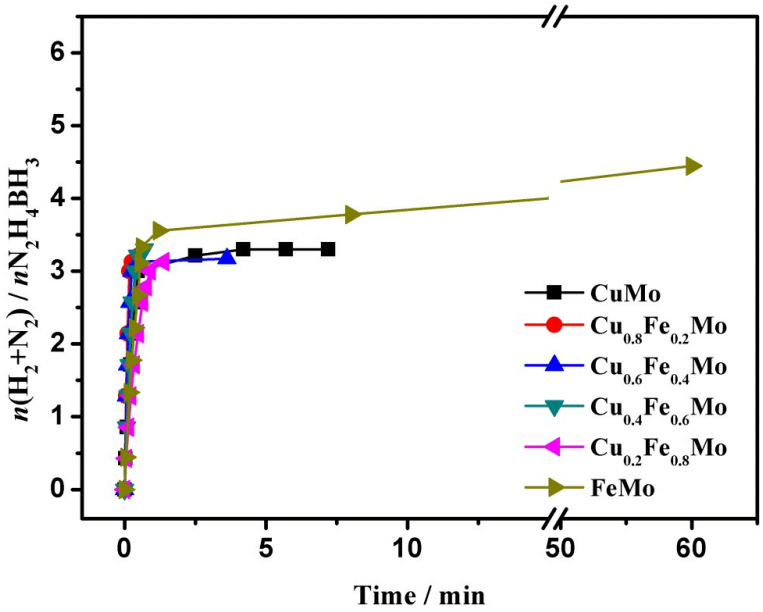

Fig. S12 Time-course plots for the dehydrogenation of $N_2H_4BH_3$ aqueous solution (0.2 M, 5 mL) catalyzed by $Cu_{1-y}Fe_yMo$ NPs with different compositions of Cu and Fe in the presence of NaOH (2.0 M) at 323 K ($n_{metal}/n_{N_2H_4BH_3}$ = 0.2).

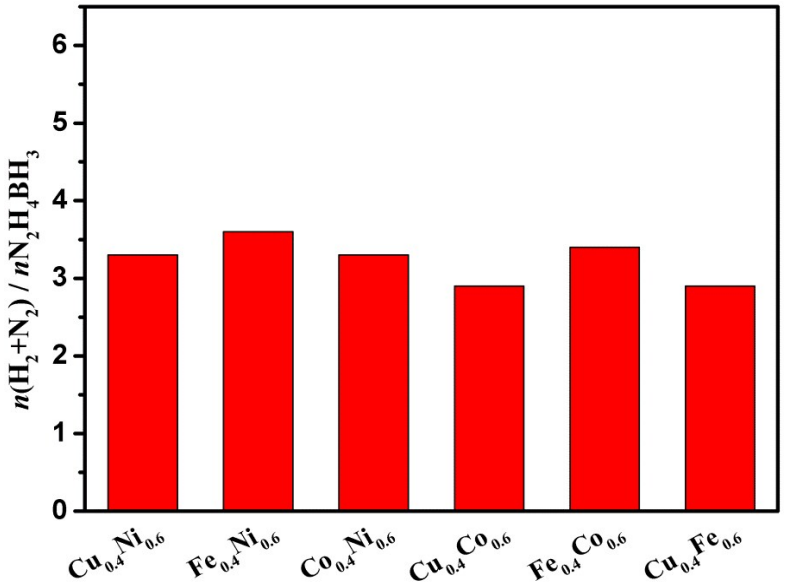

Fig. S13 Time-course plots for the dehydrogenation of $N_2H_4BH_3$ aqueous solution (0.2 M, 5 mL) catalyzed by different catalysts in the presence of NaOH (2.0 M) at 323 K ($n_{metal}/n_{N_2H_4BH_3}$ = 0.1).

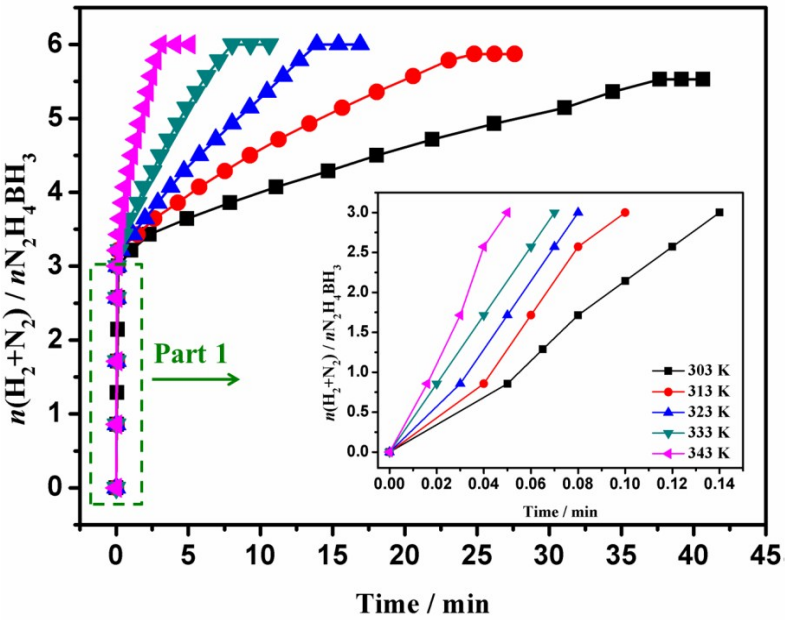

Fig. S14 Time-course plots for the dehydrogenation of $N_2H_4BH_3$ aqueous solution (0.2 M, 5 mL) catalyzed by $Cu_{0.4}Ni_{0.6}Mo$ catalysts in the presence of NaOH (2.0 M) at different temperatures ($n_{metal}/n_{N_2H_4BH_3}$ = 0.2). Inset shows the enlarged region with part 1 to see clearly.

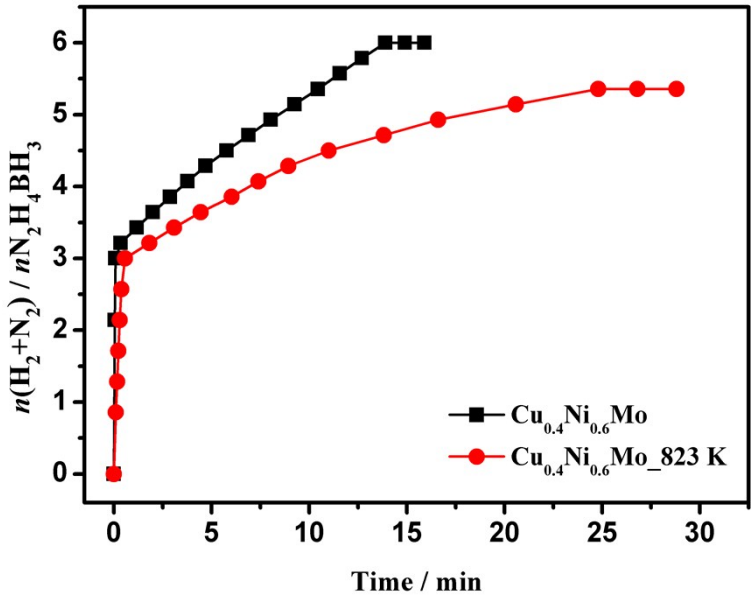

Fig. S15 Time-course plots for the dehydrogenation of $N_2H_4BH_3$ aqueous solution (0.2 M, 5 mL) catalyzed by $Cu_{0.4}Ni_{0.6}Mo$ NPs before and after heat treatment at 823 K in the presence of NaOH (2.0 M) at 323 K ($n_{metal}/nN_2H_4BH_3$ = 0.2).

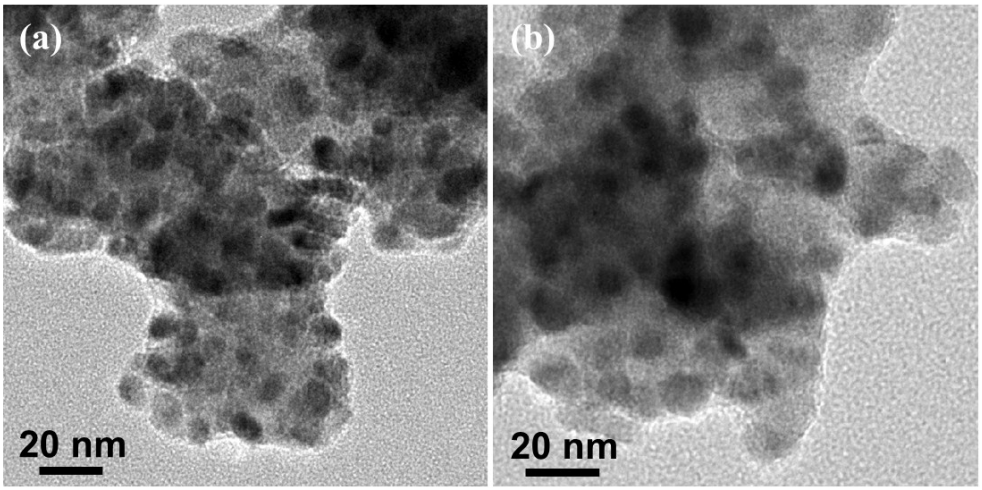

Fig. S16 (a,b) TEM images of $Cu_{0.4}Ni_{0.6}Mo$ NPs after heat treatment at 823 K for 3 h under Ar atmosphere in tube furnace.

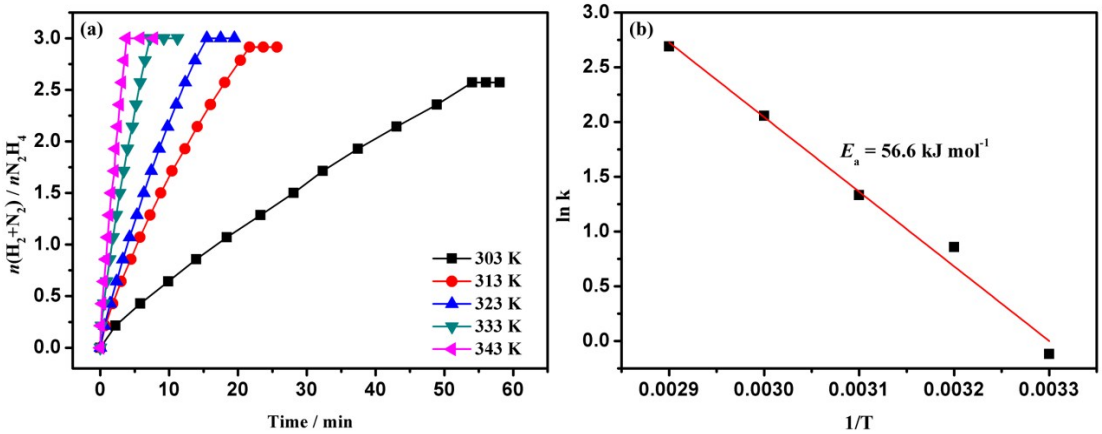

Fig. S17 (a) Time-course plots for the dehydrogenation of $N_2H_4 \cdot H_2O$ aqueous solution (0.2 M, 5 mL) catalyzed by $Cu_{0.4}Ni_{0.6}Mo$ catalysts in the presence of NaOH (2.0 M) at different temperatures ($n_{metal}/n_{N_2H_4}$ = 0.2). (b) The corresponding Arrhenius plot.

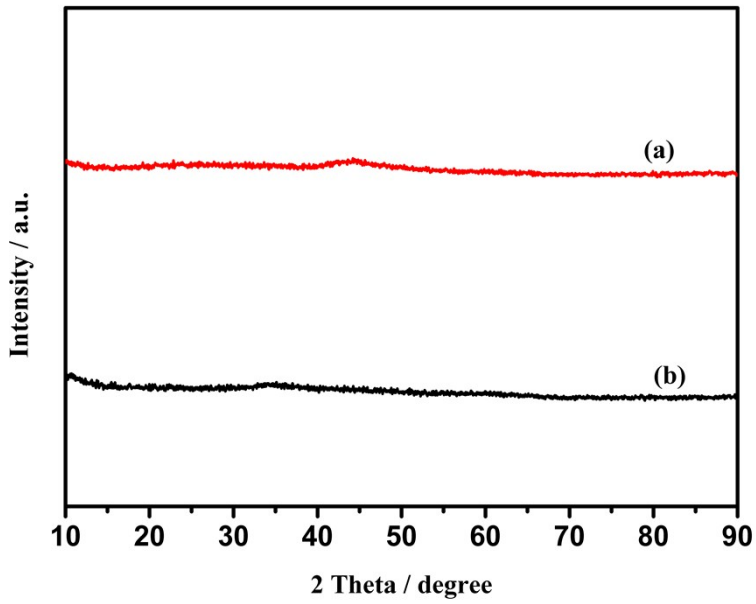

Fig. S18 X-ray diffraction patterns of $Cu_{0.4}Ni_{0.6}Mo$ NPs (a) before and (b) after the durability test.

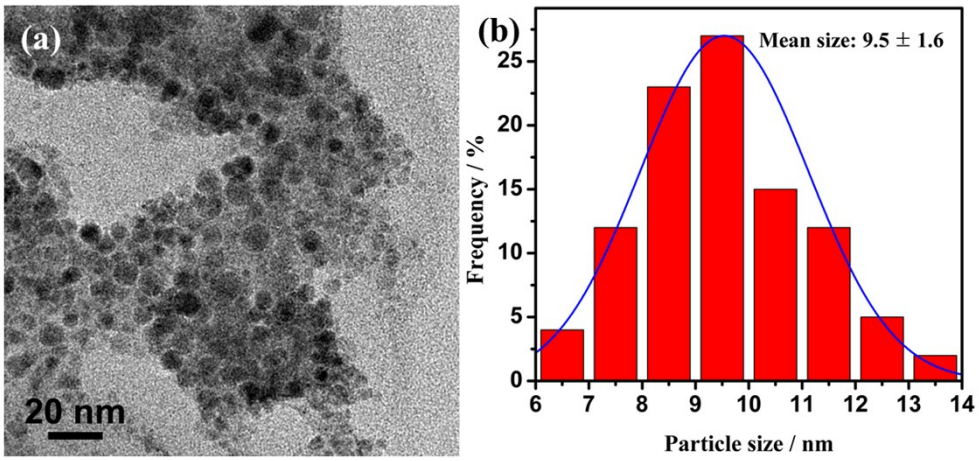

Fig. S19 (a) TEM image and (b) the corresponding particle size distribution of $Cu_{0.4}Ni_{0.6}Mo$ NPs after the durability test.